

# Trade-off between the control bandwidth and the measurement accuracy in Atomic Force Microscopy

Stefan Kuiper, Paul Van den Hof  
Delft Center for Systems and Control  
Delft University of Technology  
Mekelweg 2, 2628 CD, Delft, The Netherlands.  
Email: stefan.kuiper@tudelft.nl, p.m.j.vandenhof@tudelft.nl

Georg Schitter  
Automation and Control Institute  
Vienna University of Technology  
Gusshausstrasse 27-29, A-1040, Vienna, Austria.  
Email: schitter@acin.tuwien.ac.at  
(corresponding author)

**Abstract**—In Atomic Force Microscopy the force between the tip and the sample is controlled in a feedback loop in order to prevent damage to the tip and the sample during scanning, and also to convert the force measurement into an estimate of the sample topography. In this paper it is experimentally shown that, due to the dynamical uncertainty of the systems, in the control design a direct trade-off has to be made between the bandwidth of the feedback loop on the one hand and the accuracy of the topography estimation on the other hand.

## I. INTRODUCTION

In Atomic Force Microscopy (AFM) [1], the sample topography is measured by probing the sample with a very sharp tip, while scanning the sample or tip in a raster scan-pattern. The measurement tip is mounted on the free end of a micro-cantilever which allows to measure the interaction force between the tip and the sample during imaging. The nonlinear tip sample interaction force is controlled in a feedback loop for two reasons: (i) to prevent damage of the tip and the sample during imaging, and (ii) to provide an estimate of the sample topography. In order to provide the scanning motion and to allow the control of the tip sample force, a positioning stage is used which can position the tip relative to the sample in all three spatial directions.

A major challenge in AFM development is to improve its relatively low-imaging speed, taking in the order of several minutes per frame for most commercially available systems nowadays [2]. This has motivated a vast amount of research on improving both the achievable scanning speed, as well as improving the bandwidth of the feedback loop that controls the tip sample interaction force [3], [4], [5], [6]. Meanwhile, the consequences of the increased control bandwidth on the accuracy of the instruments has not been investigated in much detail. Improved topography estimation has been investigated by taking into account a model of the dynamical behavior of the system [7], [8]. However, the dynamical behavior of the system may show some variations when changing the tip, sample or imaging conditions, which poses strong limitations on the achievable control bandwidth and the accuracy of the topography estimation. Recently, a new method has been proposed for integrated design of the feedback controller and topography estimator, while taking into account the dynamical uncertainties of the system [9]. In this contribution, the appli-

cation of the integrated design method of [9] is demonstrated on a commercially available AFM system, and the influence of the dynamical uncertainty of the system on the topography estimation accuracy experimentally validated.

Section II discusses the topography estimation problem, and how the accuracy of the topography estimation depends on the design of the feedback controller. This is discussed and analyzed for a commercially available AFM in Section III. Experimental validation is shown in Section IV, and conclusions are drawn in Section V.

## II. TOPOGRAPHY ESTIMATION IN AFM

Figure 1 shows a block diagram of the feedback loop in AFM, with  $G$  the actuator dynamics,  $P$  the sensor dynamics, and  $K$  the feedback controller. While scanning, the sample topography enters the feedback loop as an unknown disturbance signal denoted  $h(t)$  in Figure 1. The feedback controller is tracking this topography variation via the actuator. In Laplace domain this is given as:

$$X(s) = -\frac{L(s)}{1 + L(s)} \cdot H(s) = E(s) - H(s); \quad (1)$$

with  $L(s) = P(s) \cdot K(s) \cdot G(s)$  the loop gain of the control loop.  $H(s)$ ,  $X(s)$  and  $E(s)$  are the Laplace transforms of the topography signal  $h(t)$ , the actuator displacement  $x(t)$ , and the control error  $e(t)$  respectively.

In most commercially available AFM-systems a calibrated scaling of the control signal  $u(t)$  is taken as a measure of the sample topography. However, for higher bandwidth and more accurate sample topography estimation the cantilever deflection signal  $d(t)$ , and the system dynamics should be taken into account [7], [8]:

$$\hat{H}(s) = \underbrace{\hat{P}^{-1}(s) \cdot D(s)}_{\hat{E}(s)} - \underbrace{\hat{G} \cdot U(s)}_{\hat{X}(s)}, \quad (2)$$

with  $\hat{P}(s)$  a model of the sensor dynamics  $P(s)$ , and  $\hat{G}(s)$  a model of the actuator dynamics  $G(s)$ . Combining (1) and (2),

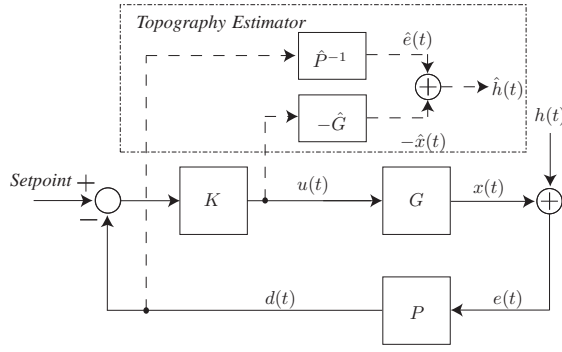


Figure 1. Block diagram of the vertical feedback loop in AFM, with actuator dynamics  $G$ , sensor dynamics  $P$ , and feedback controller  $K$ . The topography estimator provides an estimate of the topography signal  $\hat{h}(t)$  based on sensor signal  $d(t)$  and control signal  $u(t)$ .

the topography estimation error can be calculated as:

$$\begin{aligned}
 \varepsilon(s) &= \hat{H}(s) - H(s) = [\hat{E}(s) - E(s)] - [\hat{X}(s) - X(s)] \\
 &= [\hat{P}(s)^{-1} \cdot D(s) - E(s)] - [\hat{G}(s) \cdot U(s) - X(s)] \quad (3) \\
 &= \frac{[P(s)\hat{P}^{-1}(s) - 1] - P(s)K(s)[\hat{G}(s) - G(s)]}{1 + L(s)} \cdot H(s),
 \end{aligned}$$

This transfer function reveals that the topography estimation error is partly stemming from the modeling error of the sensor dynamics  $[P(s) \cdot \hat{P}^{-1}(s) - 1]$ , and partly stemming from the modeling error of the actuator dynamics  $[\hat{G}(s) - G(s)]$ . Important is also to note the influence of the feedback controller  $K(s)$  in Equation (3), determining the propagation of the modeling errors towards the topography estimation error.

A difficulty in the modeling of the system dynamics is that some dynamic variations may occur when changing the sample, measurement tip, or the imaging conditions. As a consequence, the system contains some dynamical uncertainty which limits the achievable accuracy of the topography estimate. Recently, an integrated design methodology is proposed to design the feedback controller  $K(s)$  and topography estimator model  $\hat{G}(s)$ , explicitly taking into account the influence of the dynamical uncertainty of the system [9]. In the following this integrated design strategy is applied on a commercially available AFM system, and experimentally validated via two design cases with different control bandwidths.

### III. DESIGN EXAMPLE AND ANALYSIS

The experimental setup used in this research is based on a commercially available AFM-system (Multimode V, Bruker Nano Inc., Santa Barbara, USA), which utilizes a piezoelectric tube scanner ('J-scanner') to position the sample in all three spatial directions. In order to identify the dynamical behavior of the system and its variations, the system is prepared several times using different sample discs with masses ranging from 0.5 to 1 gram, and by varying the alignment of the sample disc on the actuator. The actuator responses are measured by using a network analyzer (4395A, Agilent, Santa Clara, USA). By only using cantilevers with high free resonance frequencies

( $\geq 300$  kHz) in contact mode, the sensor dynamics can be considered static below 100 kHz, which is the frequency range of interest. Therefore, the sensor dynamics  $P$  are neglected in the following analysis, and for convenience the gain from actuator input  $u(t)$  to cantilever deflection signal  $d(t)$  is normalized. The results of two different frequency response measurements are shown in Figure 2a (solid, red and dashed blue, lines), showing the first longitudinal resonance of the piezoelectric tube scanner at 8 kHz. The various measurements clearly reveal the variations in the dynamical behavior associated with the different load conditions.

For the model-based controller design a 7th order dynamical model  $G_n(s)$  is fitted based on the data of 12 different frequency response measurements, to capture the nominal dynamical behavior of the system, as is shown by the dashed-dotted lines of Figure 2. Based on this nominal model the maximum multiplicative modeling error can be determined at each frequency point

$$\Psi(\omega_f) = \max_{j=1 \dots k} \left| \frac{\Phi_j(\omega_f) - G_n(\omega_f)}{G_n(\omega_f)} \right|, \quad (4)$$

with  $\Phi_j(\omega_f)$  the  $j^{\text{th}}$  measured frequency response of the actuator dynamics, and with  $j = 1 \dots k$  the number of frequency response measurements. The maximum multiplicative modeling error is shown by the solid line of Figure 2b, and shows that the dynamical uncertainty tends to become larger at higher frequency. To capture the dynamical uncertainty into the model set a 5th order overbounding filter  $Q(s) \geq \Psi(\omega_f)$  is fitted as shown by the dashed line of Figure 2b. As discussed in [9] the accuracy of the topography estimate can be explicitly addressed in the design of the feedback controller by penalizing the excitation of the dynamical uncertainties of the system, governed by weighting filter  $Q(s)$ . In the sequel of the paper two design cases are compared, both designed according to the design procedure of [9]: one design case denoted 'LB' in which higher emphasis is put on the accuracy of the topography estimate, and one design case denoted 'HB' in which the control bandwidth is considered more important. Figures 3a shows the Bode magnitude plots of the nominal sensitivity function for both design cases, with a disturbance rejection bandwidth of about 400 Hz for design case LB (solid, black), and 1 kHz for design case HB (dashed, red). Meanwhile, Figure 3b shows the worst-case magnitude of the transfer towards the topography estimation error  $\frac{\varepsilon(\omega_f)}{H(\omega_f)}$  analyzed at each frequency point for both design cases. These graphs are obtained by substituting the designed feedback controller  $K$ , the model of the nominal actuator dynamics  $\hat{G}$ , and frequency response measurements  $\Phi_n(\omega_f)$  into Equation 3, and assuming the sensor dynamics to be static and normalized  $\hat{P} = P = 1$ :

$$\max \left| \frac{\varepsilon(\omega_f)}{H(\omega_f)} \right| = \max_{j \in [1 \dots k]} \left| \frac{K(\omega_f)[\Phi_j(\omega_f) - \hat{G}(\omega_f)]}{1 + K(\omega_f)\Phi_j(\omega_f)} \right|.$$

Figures 3 shows that for design case LB the accuracy of the topography estimate is better as compared design case HB, particularly at higher frequency. This is explained by the

fact that with the lower control bandwidth in design case *LB*, also the excitation of the uncertain dynamics is lower, which improves the accuracy of the topography estimation. Hence, Figures 3 clearly reveals the design trade-off between the control bandwidth of the system, and the accuracy of the topography estimate.

#### IV. EXPERIMENTAL RESULTS

In order to demonstrate the trade-off between the bandwidth and the accuracy of the system experimentally, the feedback controllers are implemented on the physical system by means of a *Field-Programmable-Gate-Array* (FPGA, Virtex-II Pro XtremeDSP Development Kit, Nallatech, Camarillo CA, USA). In order to facilitate the implementation, the 15th order controllers obtained from the controller synthesis are reduced to 10th and 8th order for the lower and higher bandwidth designs respectively. The controllers are discretized to a sampling rate of 260 kHz, and implemented on the *FPGA* in a biquad structure. The implementation of the (model-based) topography estimator is done offline, by recording the signals via the data channels of the Nanoscope V controller, and filtering the data with the designed estimator model in Simulink of matlab.

In order to isolate the topography estimation errors stemming from the dynamical uncertainty of the system from other error sources such as the scanner drift in the lateral plane, an arbitrary topography signal is added to the sensor signal using an analog summing amplifier, while the scanning motion of the system is disabled. As the applied topography signal is fully known, this allows to accurately judge the topography estimation errors with the different feedback controllers and topography estimators.

Figure 4 shows the measured results when applying a 200 Hz block wave signal with an amplitude of 250 nm as a topography signal to the system controlled with either the low bandwidth or the high bandwidth feedback controller. Figure 4 shows the output of the feedback controller  $u(t)$  (Fig. 4a), the measured tracking error signal from the photodiode  $d(t)$  (Fig. 4c), the estimated sample topography  $\hat{h}(t)$  (Fig. 4b), and the topography estimation error  $\epsilon(t) = \hat{h}(t) - h(t)$  (Fig. 4d), for the systems corresponding to both design cases. The graphs of Figure 4a and 4c clearly reveal that the system controlled by the high bandwidth controller (design case *HB*) provides a better tracking of the topography signal. These experiments are repeated several times (data not shown), while varying the load conditions on the scanner, showing that for this topography signal the RMS value of the tracking error is about 30% lower with design case *HB*. In contrast, Figure 4d reveals that with design case *LB* the topography estimation errors are significantly smaller (40% RMS) as compared to design case *HB*. Hence, the results of Figure 4 clearly confirm the trade-off between the tracking bandwidth, and the accuracy of the topography estimate. Analyzing the periodicity of the topography estimation error reveals that a significant fraction of the topography estimation error is stemming from the dynamical uncertainty around the lateral resonance at 1 kHz,

which confirms the frequency domain analysis of the dynamic uncertainty shown in Figure 3b.

#### V. CONCLUSIONS

In this contribution it is experimentally demonstrated that the uncertain dynamics in AFM require a design trade-off between the disturbance rejection bandwidth of the instrument, and the guaranteed bounds on the topography estimation error (i.e. the accuracy of the instrument). Therefore, in designing the feedback controller in AFM the intended imaging applications of the instrument has to be considered. When imaging for instance fragile biological samples, minimizing the force variations between the tip and the sample may be most important in order not to damage the sample, aiming for an as high as possible control bandwidth and therefore the requirements on the accuracy of the topography estimation may be relaxed. However, in other application such as quality assurance in the semiconductor industry, higher emphasis might be given on the quality of the topography estimation. Samples from material science or potentially semiconductors are not as fragile as biological systems, and higher importance may be given to the metrological aspects of the instrument. The integrated design method demonstrated in this contribution can be used to handle this design trade-off and optimize the feedback controller and topography estimator of the system to the particular imaging application. These results also indicate that the consistence of the dynamical behavior of the system may be an important design criterion for future AFM development in order to allow both fast and accurate AFM imaging. Future work includes the development of a method to explicitly address the hysteresis of the piezo-actuator in the estimation of the sample topography to further improve the accuracy of the instrument.

#### REFERENCES

- [1] G. Binnig, C. Quate, and C. Gerber, "Atomic force microscope," *Phys. Rev. Lett.*, vol. 56, no. 9, pp. 930–933, 1986.
- [2] P. Hansma, G. Schitter, G. Fantner, and C. Prater, "High speed atomic force microscopy," *Science*, vol. 314, pp. 601–602, 2006.
- [3] T. Ando, N. Kodera, E. Takai, D. Maruyama, K. Saito, and A. Toda, "A high-speed atomic force microscope for studying biological macromolecules," *Proc. Nat. Acad. Sci.*, vol. 98, no. 22, pp. 12468–12472, 2001.
- [4] G. Schitter, K. Aström, B. DeMartini, P. Thurner, K. Turner, and P. Hansma, "Design and modeling of a high-speed afm-scanner," *IEEE Trans. Control Syst. Technol.*, vol. 15, pp. 906–915, 2007.
- [5] S. Devasia, E. Eleftheriou, and S. Moheimani, "A survey of control issues in nanopositioning," *IEEE Trans. Control Syst. Technol.*, vol. 15, pp. 802–823, 2007.
- [6] J. Butterworth, L. Pao, and D. Abramovitch, "A comparison of control architectures for atomic force microscopes," *Asian J. Control*, vol. 11, no. 2, pp. 175–181, 2009.
- [7] G. Schitter, P. Menold, H. Knapp, F. Allgöwer, and A. Stemmer, "High performance feedback for fast scanning atomic force microscopes," *Rev. Sci. Instrum.*, vol. 72, p. 3320, 2001.
- [8] S. Salapaka, T. De, and A. Sebastian, "A robust control based solution to the sample-profile estimation problem in fast atomic force microscopy," *Int. J. Robust Nonlin. Control*, vol. 15, no. 16, pp. 821–838, 2005.
- [9] S. Kuiper, P. Van den Hof, and G. Schitter, "Towards integrated design of a robust feedback controller and topography estimator for atomic force microscopy," in *IFAC World Congress*, vol. 18, no. 1, 2011, pp. 12709–12714.

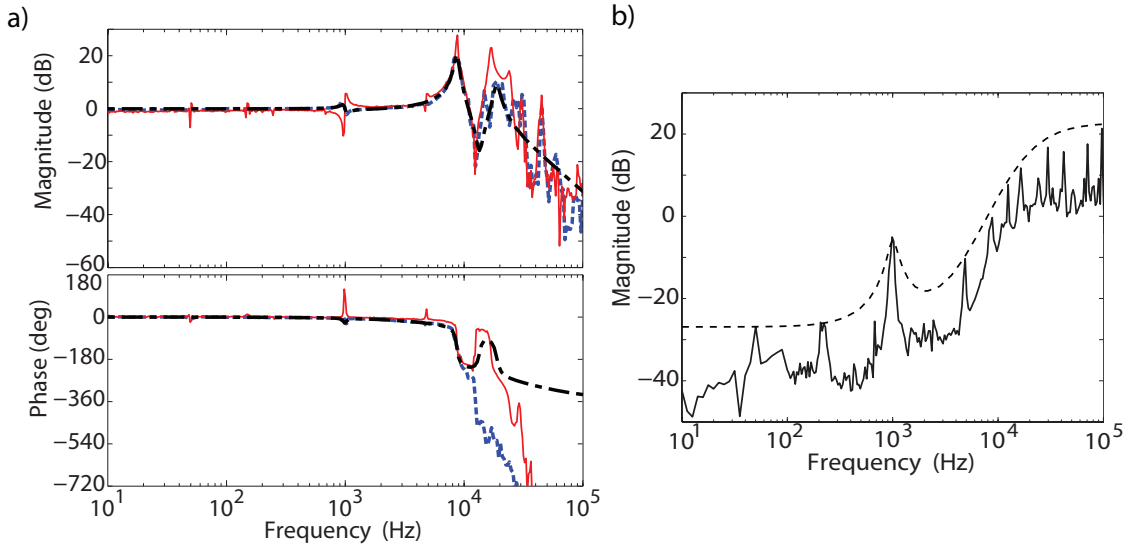


Figure 2. (a) Frequency response of the tube scanner measured in two different identification experiments (solid, red), and (dashed blue), and the frequency response of the 7th order model (dashed-dotted, black) (b) the maximum multiplicative model error (solid, black), and the error over-bounding filter  $Q(s)$  (dashed, black).

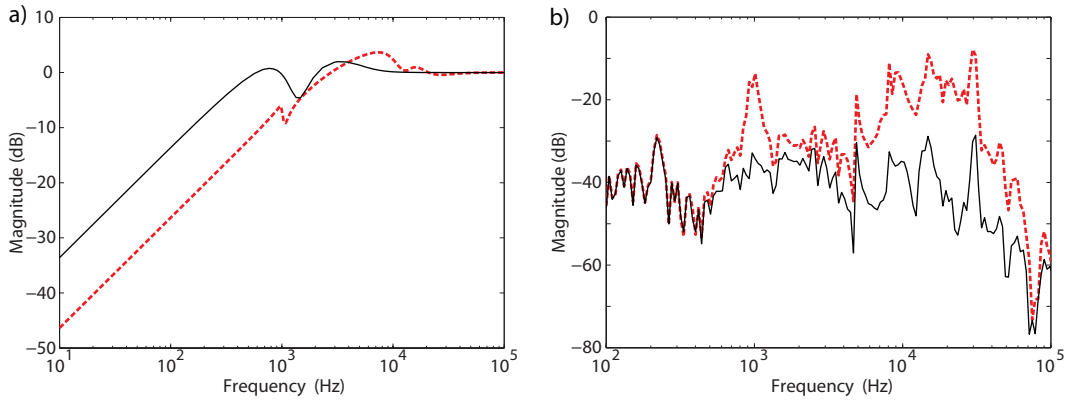


Figure 3. Frequency response plot of the nominal sensitivity function (a), and the worst-case topography estimation error determined at each frequency point for the closed-system (b), for design case  $LB$  (solid, black), and design case  $HB$  (dashed, red).

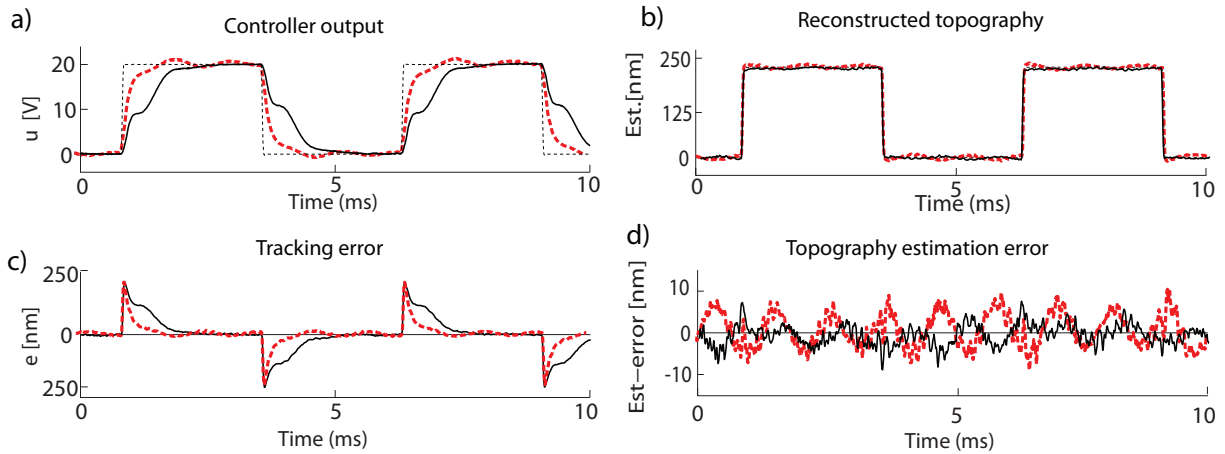


Figure 4. System outputs when applying a 200 Hz, 250 nm block wave signal as an artificial topography signal, for the system with a low-bandwidth controller (design case  $LB$ , solid, black lines), and for system with a high bandwidth controller (design case  $HB$ , dashed, red lines). Figure (a) shows the applied artificial reference signal  $h(t)$  (dashed, black) together with the output of the feedback controller  $u(t)$ , while figure (c) shows the measured control error  $d(t)$ . Figure (b) shows the outputs of the topography estimator  $\hat{h}$ , and Figure (d) show the topography estimation error  $\epsilon(t) = \hat{h}(t) - h(t)$ .